Cu doping effects on the electronic structure of $Fe_{1-x}Cu_xSe$

S. Huh [1,2,*] Z. Lu [3,4,*] Y. S. Kim,[1,2] D. Kim [1,2] S. B. Liu,[3,4] M. W. Ma,[3,5] L. Yu,[3,4,5,†] F. Zhou,[3,4,5] X. L. Dong [3,4,5]
C. Kim,[1,2,‡] and Z. X. Zhao[3,4,5]

[1]*Department of Physics and Astronomy, Seoul National University (SNU), Seoul 08826, Republic of Korea*
[2]*Center for Correlated Electron Systems, Institute for Basic Science (IBS), Seoul 08826, Republic of Korea*
[3]*Beijing National Laboratory for Condensed Matter Physics and Institute of Physics, Chinese Academy of Sciences, Beijing 100190, China*
[4]*School of Physical Sciences, University of Chinese Academy of Sciences, Beijing 100049, China*
[5]*Songshan Lake Materials Laboratory, Dongguan, Guangdong 523808, China*

Using angle-resolved photoemission spectroscopy, we investigated the evolution of the electronic structure of $Fe_{1-x}Cu_xSe$ from $x = 0$ to 0.10. We found that the substitution of Fe by Cu introduces extra electron carriers. The hole bands near the Γ point were observed to shift downward with increasing doping x and completely sank down below the Fermi level (E_F) for $x \geqslant 0.05$. Meanwhile, the electron pockets near the M point became larger but lost the spectral weight near E_F. Concomitantly, the effective mass of the electron bands increased with doping. Our results show how a metal-insulator transition behavior occurs upon Cu doping in view of the electronic structure and provide a platform to further investigation on the origin of emergent magnetic fluctuation in $Fe_{1-x}Cu_xSe$.

I. INTRODUCTION

Chemical substitution or doping studies have been widely conducted on correlated materials to control the electronic structure as well as physical properties. For example, it can change the chemical pressure, electron correlation, Fermi energy, and carrier density. As such, investigating the chemical substitution effects can provide critical clues to understanding the underlying mechanism for various phenomena such as emergent magnetism, metal-insulator transition (MIT), spin/charge density waves, and superconductivity [1–7].

Numerous chemical substitution studies have been performed on iron-based superconductors (IBSs) to understand the superconductivity and the interplay between the superconductivity and emergent phenomena [8,9]. Among IBSs, FeSe is a system for which chemical substitution studies have been intensively done. The resultant changes in the electronic, magnetic, and superconducting properties through doping have provided rich insights into the underlining nature of the superconductivity. Moreover, exotic phenomena such as Bardeen-Cooper-Schrieffer to Bose-Einstein condensation crossover and topological superconductivity have been observed in substituted $FeSe_{1-x}S_x$ and $FeSe_{1-x}Te_x$ systems [10–13]. While these studies have expanded the boundary of the rich physics in FeSe, most of the studies have been limited to the substitution of Se with isovalent atoms. There are relatively less substitution studies on the Fe site

due to the challenge of synthesizing high-quality single crystals.

Investigating the Fe-site substitution may provide new opportunities for a better understanding of superconductivity and exploration of emergent phenomena. Cu-doped FeSe is a suitable candidate to perform such studies because of the recent success of high-quality single crystal synthesis [14]. Previous studies on Cu-doped FeSe have reported that the structural transition and superconductivity are suppressed by a small amount of Cu doping and that an MIT-like behavior appears with further doping [14,15]. This unexpected MIT in FeSe calls for systematic spectroscopic studies on the Cu doping effect [16]. In addition, emergence of magnetic fluctuation [17] and restoration of the critical temperature T_c near 30 K under hydrostatic pressure [18] make the $Fe_{1-x}Cu_xSe$ system even more interesting and ask for deeper understanding of its properties at the microscopic level. In elucidating the Cu doping effect and mechanism of emergent phenomena, the electronic structure information should be vital but has been lacking so far.

In this work, we report results of a systematic angle-resolved photoemission spectroscopy (ARPES) study on $Fe_{1-x}Cu_xSe$ ($x = 0$, 0.02, 0.03, 0.05, and 0.10) to investigate the electronic structure. It is found that Cu substitution accompanies an effective electron doping; the size of the hole (electron) pocket near the Γ (M) point decreases (increases) with doping. In addition, for the electron bands near the M point, the near E_F spectral weight is reduced while the effective mass increases, which shows how MIT is realized in terms of the electronic structure. Our work is the first to report the detailed electronic structure evolution of the $Fe_{1-x}Cu_xSe$ system and may lay a platform to future studies on the origin of the emergent magnetic fluctuation in this doping range.

———————
*These authots contributed equally to this work.
†li.yu@iphy.ac.cn
‡changyoung@snu.ac.kr

(a)

(b)
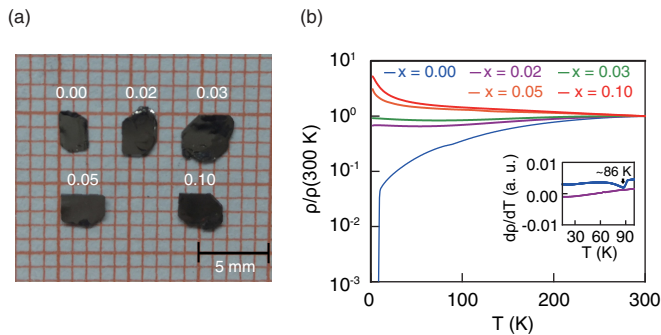
FIG. 1. (a) Optical image of $Fe_{1-x}Cu_xSe$ single crystals. (b) Temperature-dependent resistivity between 2 and 300 K. The inset shows the derivative of the resistivity for $x = 0$ and 0.02 as a function of the temperature. The black arrow indicates a structural transition (T_s).

II. EXPERIMENT

High-quality single crystals of $Fe_{1-x}Cu_xSe$ were synthesized by the chemical vapor transport method using a mixture of $AlCl_3$ and KCl as the transport agent [14]. In-plane electrical transport measurements were performed with a Quantum Design PPMS-9 system. ARPES measurements were performed using a home-laboratory-based system at Seoul National University. All spectra were acquired using a VG-Scienta electron analyzer and a discharge lamp from Fermi instruments. A photon energy of 21.218 eV was used in the experiment. The instrumental energy resolution was better than 20 meV. Samples were cleaved in an ultrahigh vacuum at less than 8×10^{-11} Torr. To minimize the aging effect, all data were taken within 10 h after cleaving.

III. RESULTS AND DISCUSSION

Figure 1(a) shows an optical image of $Fe_{1-x}Cu_xSe$ single crystals. Sizable single crystals with various doping concentrations were obtained and used in our ARPES experiments. The chemical composition of crystals was determined by inductively coupled plasma atomic emission spectroscopy. Temperature-dependent in-plane resistivity for various dopings is shown in Fig. 1(b). Consistent with previous results [14,15], the critical temperature T_c and the structural transition temperature T_s are completely suppressed when Cu is only slightly doped ($x < 0.02$). For a better comparison, we plot the first derivative of the resistivity in the inset. There is an anomaly near 86 K for the $x = 0$ sample which indicates T_s, while no signature of such anomaly is observable for $x = 0.02$. A heat-capacity measurement shows a consistent T_s value [14]. In addition to the suppression of the phase transition, MIT-like behavior is observed in the doping-dependent resistivity data. An upturn in the resistivity curve is observed for $x = 0.05$ and 0.10, while metallic behavior is observed over the entire temperature range for lower doping concentrations. Similar MIT behavior is reported for Cu-doped iron pnictide systems [19,20], which implies that the Cu doping effect may be universal in IBSs.

We performed ARPES experiments to investigate the Cu doping effect on the electronic structure of $Fe_{1-x}Cu_xSe$.

Figures 2(a)–2(e) show Fermi surface maps of $Fe_{1-x}Cu_xSe$ for different Cu concentrations. FeSe data were taken at 100 K to avoid the change in the band structure from the nematic phase transition which occurs near 90 K [21], while other data were taken at 20 K since no structural transition is observed for these concentrations as mentioned above. This allows us to systematically compare the band structures of $Fe_{1-x}Cu_xSe$ with various x values. With increasing Cu doping, the hole pockets near the Γ point gradually get smaller and eventually disappear for $x > 0.05$. On the other hand, the size of the electron pockets near the M_1 and M_2 points increases. The overall change of the Fermi surface topology suggests that Cu substitution dopes electrons in the FeSe system. A number of studies reported that Cu doping to IBSs may result in hole doping [22,23]. Especially at low temperature, the Hall coefficient changes from a negative number for the pristine FeSe to a positive number for Cu-doped FeSe, suggesting hole-dominant carrier properties in transport properties [14,15]. However, our result shows an electron doping behavior in $Fe_{1-x}Cu_xSe$ as observed for the cases $Ba(Fe_{1-x}Cu_x)_2As_2$ and $NaFe_{1-x}Cu_xAs$ [24–26]. At present, it appears to be difficult to find a simple explanation for this discrepancy in the carrier property from the two methods and further investigation is needed to resolve the issue. Meanwhile, the overall shape of the electron pockets becomes more circular in comparison to the two perpendicularly crossing elliptical-shaped Fermi surface pockets of the pristine FeSe (inset of Fig. 2 and Supplemental Material [27]). These large circular electron pockets with the absence of the hole pockets at the Γ point suggests an interesting similarity to the Fermi surface topology of heavily electron-doped FeSe systems such as intercalated FeSe [28] and one monolayer FeSe grown on $SrTiO_3$ [29].

In order to illustrate the evolution of the electronic structure in detail, we compare band dispersions along a high-symmetry direction. Figures 3(a) and 3(b) show a high-symmetry cut of FeSe near the Γ point and its schematic electronic structure, respectively. Similar to the results of previous FeSe studies [30–32], the so-called α- and β-hole bands with $d_{xz/yz}$ orbital characters and the γ band with the d_{xy} orbital can be clearly seen in our results. The effect of Cu doping is well resolved in these high-symmetry cut data [Figs. 3(c)–3(f)] and their corresponding second-derivative spectra [Figs. 3(g)–3(j)]. The data clearly show that hole bands shift downward with doping. Especially, the α-hole band locates completely below E_F from $x \geqslant 0.05$, resulting in a strong reduction in the near E_F spectral weight. The temperature dependence of the $x = 0.05$ and 0.10 data (Supplemental Material [27]) shows that the downward shift of the α-hole band is indeed an intrinsic property. Such dramatic change in the Fermi surface topology and the near E_F spectral weight may be at least partially responsible for the insulating behavior for $x \geqslant 0.05$. Note that the weak residual hole pocket feature near the Γ point in the Fermi surface maps of $x = 0.05$ and 0.10 in Fig. 2 is from broadening of the dispersion tail, possibly due to impurity scattering. In Figs. 3(k) and 3(l), we plot doping-dependent energy distribution curves (EDCs) at the Γ point and their second derivatives, respectively. Red, green, and blue arrows indicate the topmost energy positions of the α, β, and γ bands, respectively. A summary of the band
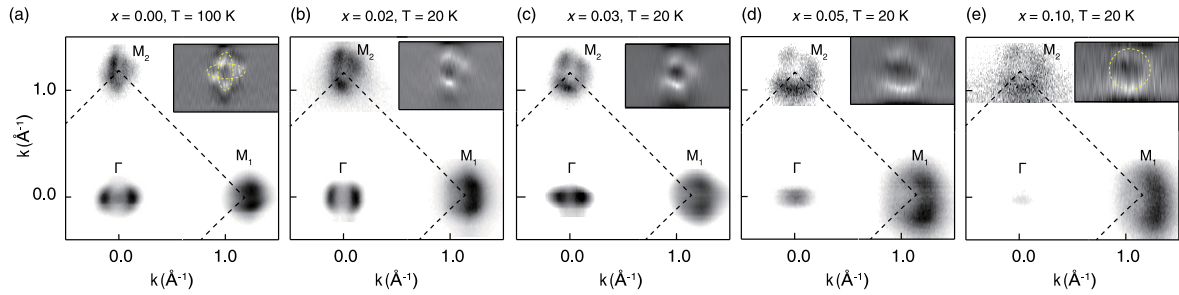
FIG. 2. (a)–(e) Fermi surface map of $Fe_{1-x}Cu_xSe$ for different Cu concentrations. The inset shows the second derivative of the Fermi surface map near the M_2 point. $x = 0$ data were taken at 100 K in order to avoid the band structure change from the nematic phase transition, while others were taken at 20 K. All the data were taken with the same ARPES spectrometer and identical experimental setting parameters.

positions is shown in Fig. 3(m) which clearly shows a downward shift for the hole bands through Cu doping. It needs to be emphasized that the doping effect appears more severe for the α and β bands compared to the γ band. In other words, $d_{xz/yz}$ orbitals are more susceptible to the electron doping than the d_{xy} orbital, implying an orbital-selective doping dependence near the Γ region.

Doping-dependent band structures around the M point are also investigated. Figures 4(a)–4(e) show high-symmetry cut data near the M_2 point measured at 20 K. We find that the

splitting of the hole band for $x = 0$ (two red dashed lines) in Fig. 4(a), a well-known spectroscopic signature for the nematic phase, is not observed anymore in data in Figs. 4(b)–4(e). This observation supports the fact that the nematic phase is suppressed upon Cu doping as mentioned above. For a better visualization, we also plotted the second-derivative spectra in Figs. 4(f)–4(j). It is seen in the data that the electron pocket
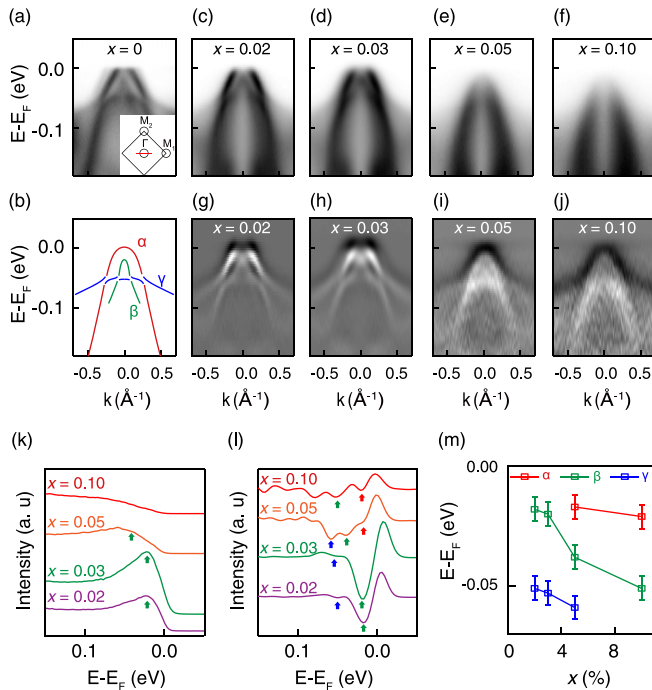
FIG. 3. (a) High-symmetry cut data taken near the Γ point at 20 K and (b) a schematic electronic structure. The inset in panel (a) schematically shows the Fermi surface pockets. The red line marks the high-symmetry cut direction. (c)–(f) High-symmetry cuts and (g)–(j) their second derivative data near the Γ point for various x. (k) Energy distribution curves (EDCs) at Γ and (l) their second derivatives. Red, green, and blue arrows indicate the positions of the α, β, and γ bands, respectively. (m) Band positions as a function of Cu concentration extracted from the EDCs plotted in panels (k) and (l).
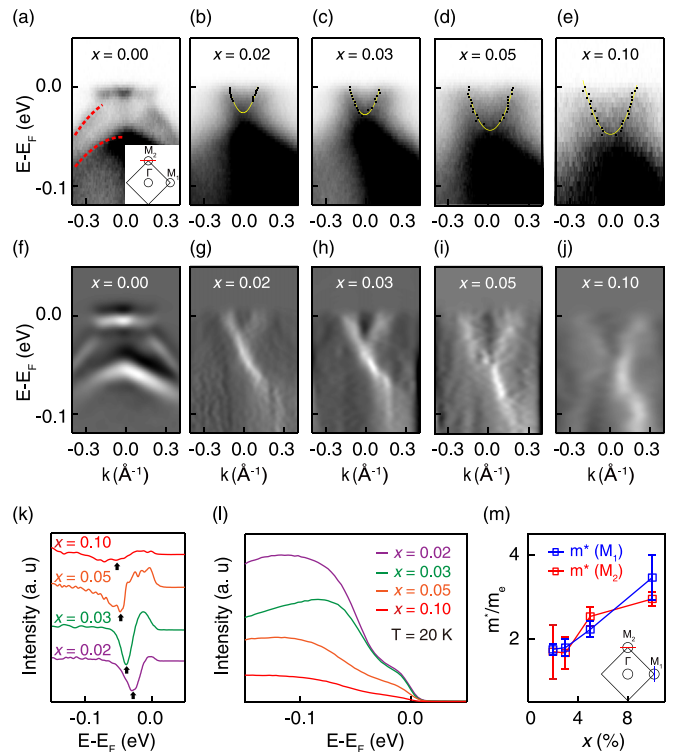
FIG. 4. (a)–(e) High-symmetry cuts near the M_2 point taken at 20 K and (g)–(j) the corresponding second derivatives. The inset in panel (a) shows a schematic Fermi surface with the high-symmetry line along which data were taken. (k) Doping-dependent second-derivative EDCs at $k = 0.0$ Å^{-1}. Black arrows mark the bottom positions of the electron bands. (l) Angle-integrated spectra near the M_2 point. A momentum integration window of $(-0.4$ Å^{-1}, 0.4 Å$^{-1})$ was used. (m) Effective mass of the electron band as a function of doping. The effective mass obtained from the M_1 (M_2) point is represented by blue (red) squares. The inset schematically shows the experimental geometry. m^* is the free electron mass.

size increases with Cu doping. It is worth noting that the two electron bands are observed for $x = 0.02$ and 0.03 even though they cannot be distinguished for $x = 0.05$ and 0.10 due to the low statistics of the data. Figure 4(k) shows doping-dependent EDCs from the second-derivative data. The black arrow indicates the bottom position of the electron band. A downward shift of the electron band through doping is clearly noted. Figure 4(l) shows angle-integrated spectra over a momentum window of $(-0.4\,\text{Å}^{-1}, 0.4\,\text{Å}^{-1})$. The near E_F spectral weight gradually decreases as Cu is doped. In addition, the effective mass of the inner electron band is determined by a parabolic fit of the dispersion as shown in Figs. 4(b)–4(e). The effective mass is almost doubled by Cu doping as seen in Fig. 4(m) (red square). Enhancement of the effective mass near the M_1 point was also observed (blue square). We double-checked it using a different fitting method and obtained the same result (see Supplemental Material [27]). As mentioned above, the electron Fermi surface pockets near the M point look similar to those of heavily electron-doped FeSe systems which also show an enhanced effective mass compared to the pristine FeSe. Especially, the effective mass for $x = 0.10$ is similar to that of one monolayer FeSe grown on SrTiO$_3$ [33]. Although Cu-doped FeSe ($x = 0.10$) has a similar Fermi surface topology and correlation to one monolayer FeSe grown on SrTiO$_3$, it lacks superconductivity, which may be due to the impurity effect from the Cu doping.

Our observations suggest that a simple momentum mixing impurity effect cannot be solely responsible for the MIT in Cu-doped FeSe. In addition to the impurity effect, the change in the Fermi surface topology through suppression of the hole pockets may be related to the insulating phase. Moreover, the enhanced correlation with the Cu doping (larger effective mass as observed for the electron bands at the M point) should also be considered. Emergence of a Mott-insulating state in heavily Cu-doped NaFeAs [19,34] may also point to the importance of electron correlation in Cu-doped FeSe systems. Assuming that each Cu substitution results in the doping of an electron, MIT appears when the total electron number of the Fe $3d$ orbital is about 6.15 [35]. Therefore, the standard Mott transition theory cannot account for the insulating state of this system because the electron filling number is not an integer [36]. Additional electronic and magnetic orders or other fac-

tors from electron correlation should trigger the transition to an insulating phase.

As for magnetism, previous studies reported that magnetic fluctuation exists from $x = 0.04$ [17]. Our data show that the hole band's top position at Γ goes below E_F at a similar Cu concentration. Thus, the origin of this magnetic fluctuation may not be solely explained within a Fermi surface nesting picture which is believed to be primarily responsible for the magnetism in IBSs [37]. Instead, Fermi surface topology change and enhanced correlation should be certainly included in theoretical models to explain the magnetism in Fe$_{1-x}$Cu$_x$Se. Concrete understanding requires further theoretical and experimental studies.

IV. CONCLUSION

We report results of a detailed electronic structure study on Fe$_{1-x}$Cu$_x$Se. We observe that the size of the hole (electron) pockets near the Γ (M) point decreases (increases) with doping. With the increase of doping, we find that the hole band's top position at the Γ point is located below E_F, which changes the overall Fermi surface topology. In addition, it is found that the effective mass of the electron band at the M point increases upon Cu doping. Our observation explains, in terms of electronic structure, why the Fe$_{1-x}$Cu$_x$Se system shows a MIT behavior and may shed light on the mechanism of the magnetic fluctuation.

[1] J. Paglione and R. L. Greene, Nat. Phys. **6**, 645 (2010).

[2] M. Imada, A. Fujimori, and Y. Tokura, Rev. Mod. Phys. **70**, 1039 (1998).

[3] B. G. Jang, G. Han, I. Park, D. Kim, Y. Y. Koh, Y. Kim, W. Kyung, H.-D. Kim, C.-M. Cheng, K.-D. Tsuei, K. D. Lee, N. Hur, J. H. Shim, C. Kim, and G. Kotliar, Nat. Commun. **12**, 1208 (2021).

[4] K. E. Wagner, E. Morosan, Y. S. Hor, J. Tao, Y. Zhu, T. Sanders, T. M. McQueen, H. W. Zandbergen, A. J. Williams, D. V. West, and R. J. Cava, Phys. Rev. B **78**, 104520 (2008).

[5] H. Miao, G. Fabbris, R. J. Koch, D. G. Mazzone, C. S. Nelson, R. Acevedo-Esteves, G. D. Gu, Y. Li, T. Yilimaz, K. Kaznatcheev, E. Vescovo, M. Oda, T. Kurosawa, N. Momono,

T. Assefa, I. K. Robinson, E. S. Bozin, J. M. Tranquada, P. D. Johnson, and M. P. M. Dean, npj Quantum Mater. **6**, 31 (2021).

[6] X. Chen, J. L. Schmehr, Z. Islam, Z. Porter, E. Zoghlin, K. Finkelstein, J. P. C. Ruff, and S. D. Wilson, Nat. Commun. **9**, 103 (2018).

[7] J. A. Sobota, Y. He, and Z.-X. Shen, Rev. Mod. Phys. **93**, 025006 (2021).

[8] Q. Si, R. Yu, and E. Abrahams, Nat. Rev. Mater. **1**, 16017 (2016).

[9] X. Chen, P. Dai, D. Feng, T. Xiang, and F.-C. Zhang, Natl. Sci. Rev. **1**, 371 (2014).

[10] S. Rinott, K. B. Chashka, A. Ribak, E. D. L. Rienks, A. T.-Ibrahimi, P. L. Fevre, F. Bertran, M. Randeria, and A. Kanigel, Sci. Adv. **3**, e1602372 (2017).

[11] T. Hashimoto, Y. Ota, A. Tsuzuki, T. Nagashima, A. Fukushima, S. Kasahara, Y. Matsuda, K. Matsuura, Y. Mizukami, T. Shibauchi, S. Shin, and K. Okazaki, Sci. Adv. **6**, eabb9052 (2020).

[12] P. Zhang, K. Yaji, T. Hashimoto, Y. Ota, T. Kondo, K. Okazaki, Z. Wang, J. Wen, G. D. Gu, H. Ding, and S. Shin, Science **360**, 182 (2018).

[13] Z. Wang, P. Zhang, G. Xu, L. K. Zeng, H. Miao, X. Xu, T. Qian, H. Weng, P. Richard, A. V. Fedorov, H. Ding, X. Dai, and Z. Fang, Phys. Rev. B **92**, 115119 (2015).

[14] H. Li, M. W. Ma, S. B. Liu, F. Zhou, and X. L. Dong, Chin. Phys. B **29**, 127404 (2020).

[15] C. Gong, S. Sun, S. Wang, and H. Lei, Phys. Rev. B **103**, 174510 (2021).

[16] Y. Mizuguchi, F. Tomioka, S. Tsuda, T. Yamaguchi, and Y. Takano, J. Phys. Soc. Jpn. **78**, 074712 (2009).

[17] S. I. Shylin, V. Ksenofontov, P. G. Naumov, S. A. Medvedev, and C. Felser, J. Supercond. Novel Magn. **31**, 763 (2018).

[18] L. M. Schoop, S. A. Medvedev, V. Ksenofontov, A. Williams, T. Palasyuk, I. A. Troyan, J. Schmitt, F. Casper, C. Wang, M. Eremets, R. J. Cava, and C. Felser, Phys. Rev. B **84**, 174505 (2011).

[19] Y. Song, Z. Yamani, C. Cao, Y. Li, C. Zhang, J. S. Chen, Q. Huang, H. Wu, J. Tao, Y. Zhu, W. Tian, S. Chi, H. Cao, Y.-B. Huang, M. Dantz, T. Schmitt, R. Yu, A. H. Nevidomskyy, E. Morosan, Q. Si *et al.*, Nat. Commun. **7**, 13879 (2016).

[20] C. Ye, W. Ruan, P. Cai, X. Li, A. Wang, X. Chen, and Y. Wang, Phys. Rev. X **5**, 021013 (2015).

[21] S. Margadonna, Y. Takabayashi, M. T. McDonald, K. Kasperkiewicz, Y. Mizuguchi, Y. Takano, A. N. Fitch, E. Suard, and K. Prassides, Chem. Commun. **2008**, 5607 (2008).

[22] Y. J. Yan, P. Cheng, J. J. Ying, X. G. Luo, F. Chen, H. Y. Zou, A. F. Wang, G. J. Ye, Z. J. Xiang, J. Q. Ma, and X. H. Chen, Phys. Rev. B **87**, 075105 (2013).

[23] V. K. Anand, P. K. Perera, A. Pandey, R. J. Goetsch, A. Kreyssig, and D. C. Johnston, Phys. Rev. B **85**, 214523 (2012).

[24] S. T. Cui, S. Kong, S. L. Ju, P. Wu, A. F. Wang, X. G. Luo, X. H. Chen, G. B. Zhang, and Z. Sun, Phys. Rev. B **88**, 245112 (2013).

[25] S. T. Cui, S. Y. Zhu, A. F. Wang, S. Kong, S. L. Ju, X. G. Luo, X. H. Chen, G. B. Zhang, and Z. Sun, Phys. Rev. B **86**, 155143 (2012).

[26] S. Ideta, T. Yoshida, I. Nishi, A. Fujimori, Y. Kotani, K. Ono, Y. Nakashima, S. Yamaichi, T. Sasagawa, M. Nakajima, K. Kihou, Y. Tomioka, C. H. Lee, A. Iyo, H. Eisaki, T. Ito, S. Uchida, and R. Arita, Phys. Rev. Lett. **110**, 107007 (2013).

[27] See Supplemental Material at http://link.aps.org/supplemental/10.1103/PhysRevB.105.245140 for additional information for data analysis and complementary experimental data.

[28] Y. Zhang, L. X. Yang, M. Xu, Z. R. Ye, F. Chen, C. He, H. C. Xu, J. Jiang, B. P. Xie, J. J. Ying, X. F. Wang, X. H. Chen, J. P. Hu, M. Matsunami, S. Kimura, and D. L. Feng, Nat. Mater. **10**, 273 (2011).

[29] S. Tan, Y. Zhang, M. Xia, Z. Ye, F. Chen, X. Xie, R. Peng, D. Xu, Q. Fan, H. Xu, J. Jiang, T. Zhang, X. Lai, T. Xiang, J. Hu, B. Xie, and D. Feng, Nat. Mater. **12**, 634 (2013).

[30] S. S. Huh, J. J. Seo, B. S. Kim, S. H. Cho, J. K. Jung, S. Kim, C. I. Kwon, J. S. Kim, Y. Y. Koh, W. S. Kyung, J. D. Denlinger, Y. H. Kim, B. N. Chae, N. D. Kim, Y. K. Kim, and C. Kim, Commun. Phys. **3**, 52 (2020).

[31] D. Liu, C. Li, J. Huang, B. Lei, L. Wang, X. Wu, B. Shen, Q. Gao, Y. Zhang, X. Liu, Y. Hu, Y. Xu, A. Liang, J. Liu, P. Ai, L. Zhao, S. He, L. Yu, G. Liu, Y. Mao *et al.*, Phys. Rev. X **8**, 031033 (2018).

[32] T. Shimojima, Y. Suzuki, A. Nakamura, N. Mitsuishi, S. Kasahara, T. Shibauchi, Y. Matsuda, Y. Ishida, S. Shin, and K. Ishizaka, Nat. Commun. **10**, 1946 (2019).

[33] D. Liu, W. Zhang, D. Mou, J. He, Y.-B. Ou, Q.-Y. Wang, Z. Li, L. Wang, L. Zhao, S. He, Y. Peng, X. Liu, C. Chen, L. Yu, G. Liu, X. Dong, J. Zhang, C. Chen, Z. Xu, J. Hu *et al.*, Nat. Commun. **3**, 931 (2012).

[34] C. E. Matt, N. Xu, B. Lv, J. Ma, F. Bisti, J. Park, T. Shang, C. Cao, Y. Song, A. H. Nevidomskyy, P. Dai, L. Patthey, N. C. Plumb, M. Radovic, J. Mesot, and M. Shi, Phys. Rev. Lett. **117**, 097001 (2016).

[35] R. Yu, H. Hu, E. M. Nica, J.-X. Zhu, and Q. Si, Front Phys. **9**, 578347 (2021).

[36] J. Kwon, M. Kim, D. Song, Y. Yoshida, J. Denlinger, W. Kyung, and C. Kim, Phys. Rev. Lett. **123**, 106401 (2019).

[37] I. I. Mazin, D. J. Singh, M. D. Johannes, and M. H. Du, Phys. Rev. Lett. **101**, 057003 (2008).